Role of cellular prion protein in mouse granulosa cells and its effects on ovarian function in knockout mice

QINYUE CAO, HEHUA WANG, JINGJING HU, YAN WANG, TONG DAI, FEN LIU, XIA YANG, QINYU YANG and CHUNHUA TU

Department of Obstetrics and Gynecology, The First Affiliated Hospital of Nanchang University, Nanchang, Jiangxi 330006, P.R. China

Received February 7, 2025; Accepted July 2, 2025

DOI: 10.3892/mmr.2025.13630

Abstract. Cellular prion protein (PrP^c) regulates ovarian reserve maintenance through anti-Müllerian hormone (AMH)-dependent mechanisms. The present study explored the role of PrP^c in the ovarian function of mice using complementary *in vitro* and *in vivo* models. First, prion protein gene (*PRNP*) knockdown or overexpression was carried out in mouse ovarian granulosa cells. *In vitro* analyses conducted using flow cytometry and ELISA revealed that the depletion of PrP^c specifically hindered the secretion of AMH compared with control groups, while the levels of progesterone (P4) and estradiol (E2) remained unchanged across all experimental groups. Importantly, the reduction in AMH levels was reversed upon re-expression of PrP^c. Additionally, neither the distribution of the cell cycle nor the rates of apoptosis were affected by the manipulation of PrP^c. Subsequently, a comparative analysis of mice with *PRNP* knockout (KO) vs. wild-type mice was performed. However, PrP^c depletion did not alter the production of progesterone or estradiol. Whilst the ovarian histology remained intact in KO mice, an elevation in follicle-stimulating hormone levels was observed, thereby suggesting a potential involvement of compensatory neuroendocrine regulation. These findings revealed that PrP^c may be a novel modulator for maintaining the ovarian reserve which depends on AMH. The present study redefined the molecular landscape of ovarian reserve depletion by identifying the dysfunction of the PrP^c-AMH axis as a possible reason for diminished ovarian reserve syndromes.

Introduction

The cellular prion protein (PrP^c) has been studied for its diverse roles across various biological systems, such as providing neuroprotection through the regulation of copper and NMDA receptors, as well as maintaining stem cell health by influencing Wnt/β-catenin signaling pathways (1-6), with particular emphasis on unraveling its mechanisms of action within the nervous system (7,8). Notably, PrP^c has been revealed to interact with amyloid-β peptides in Alzheimer's disease and α-synuclein in Parkinson's disease (9,10). Furthermore, PrP^c can modulate neuroendocrine signaling pathways, especially pathways that are associated with the regulation of gonadotropin, revealing a possible role in reproductive physiology (11,12). PrP^c is involved in oocyte maturation (13). Furthermore, in ovariectomized ewes, the expression of PrP^c in ovine uteroplacental tissues was shown to increase when the ewes were treated with estrogen and during the early stage of pregnancy (14). However, the roles of PrP^c, including how it regulates ovarian reserve maintenance and the dynamics of follicular recruitment, have not been fully elucidated.

Recent advances in reproductive endocrinology demonstrate the need to clarify the non-steroidogenic mechanisms that govern follicular homeostasis, with a particular focus on mechanisms involving anti-Müllerian hormone (AMH)-mediated signaling (15-17). As AMH levels are closely linked to ovarian reserve and are recognized as the most sensitive clinical biomarker for diminished ovarian reserve (DOR) syndromes, it is crucial to clarify the regulatory mechanisms involved (18,19). We hypothesized that PrP^c may act as a novel type of modulator for AMH-dependent follicular recruitment, potentially through mechanisms that are different from the regulation of classical steroid hormones. To test this hypothesis, two complementary models were used, the *in vitro* mouse ovarian granulosa cells (mGCs) with prion protein gene (*PRNP*) knockdown and overexpression (OE) and the *in vivo PRNP* knockout (KO) and wild-type (WT) models. The specific effects of PrP^c on AMH secretion were compared with those on progesterone (P4) and estradiol (E_2) production. The present study aimed to analyzed the effects of maintaining the follicular pool through histomorphometric analysis and reproductive longevity via litter size tracking, while also examining neuroendocrine adaptations in the HPG axis using vaginal cytology, serum FSH quantification, and ovarian reserve evaluation through follicle counting.

Materials and methods

Cell culture. mGCs were procured from Haixing Biosciences Co., Ltd. (cat. no. ORCM050). The cells were grown in

Correspondence to: Professor Chunhua Tu, Department of Obstetrics and Gynecology, The First Affiliated Hospital of Nanchang University, 17 Yongwai Zheng Street, Nanchang, Jiangxi 330006, P.R. China
E-mail: chunhuatudhj@163.com

Key words: cellular prion protein, mouse ovarian granulosa cells, ovarian function, gene knockdown, gene overexpression

high-glucose DMEM (cat. no. 12,100; Beijing Solarbio Science & Technology Co., Ltd.), which included 100 U/ml penicillin and 100 μg/ml streptomycin as standard components, with 10% heat-inactivated FBS (cat. no. FSS500; Shanghai ExCell Biology, Inc.). mGCs were maintained at 37˚C in an atmosphere with 5% CO_2, and the culture medium was replaced every 2 days. To preserve physiological relevance, cell passage was restricted to early generations (P2-P3), thereby minimizing cellular dedifferentiation. Additionally, follicle stimulating hormone receptor (FSHR) expression levels were periodically confirmed by immunofluorescence, ≥80% of cells exhibited positive FSHR staining (Fig. S1A).

Immunofluorescence. Cell coverslips were prepared by seeding 1x10^5 cells in 1 ml of medium and incubating them overnight at 37˚C with 5% CO_2 until they reached 70-80% confluency. After removing the medium, the cells were washed with ice-cold PBS and fixed using 4% paraformaldehyde (PFA) for 30 min at room temperature. Following additional washes with PBS, the cells were permeabilized with 0.5% Triton™ X-100 for 15 min and then blocked with 10% goat serum (cat. no. S9070; Beijing Solarbio Science & Technology Co., Ltd.) for 60 min at room temperature. The coverslips were then incubated overnight at 4˚C with a rabbit anti-FSHR antibody diluted to 1:200 (cat. no. 22665-1-AP; Proteintech Group, Inc.). After washing, the cells were stained with an Alexa Fluor® 488-conjugated secondary antibody at a dilution of 1:500 (cat. no. SA00006-2; Proteintech Group, Inc.) for 2 h at room temperature. Finally, the coverslips were mounted on slides using DAPI antifade medium (cat. no. S2110; Beijing Solarbio Science & Technology Co., Ltd.), and the samples were imaged for analysis using an inverted platform (Primovert LED; ZEISS, Germany).

Transfection. Recombinant lentiviruses, rLV-short hairpin (sh)RNA-Puro-m*PRNP* and rLV-m*PRNP*-3flag-ZsGreen-Puro were procured from Haixing Biosciences Co., Ltd. Empty vectors were used as negative controls (NCs). The target sequences of the *PRNP* shRNAs were as follows: m*PRNP* sh-1, 5'-GGACAACCTCATGGTGGTAGT-3'; m*PRNP* sh-2, 5'-GCGTCAATATCACCATCAAGC-3'; and m*PRNP* sh-3, 5'-GCCTATTACGACGGGAGAAGA-3'. To achieve stable silencing and OE of the *PRNP* gene, the cells were seeded into 6-well plates at a density of 2.5x10^5 cells per well, and cultured overnight until they reached a confluence of 40-50%. On the subsequent day, lentiviral transfection of the cells was performed following the protocol supplied by the manufacturer. Lentiviral vectors that encode EGFP reporters were generated using a third-generation system in 293T cells (cat. no. CL-0005; Wuhan Pricella Biotechnology Co., Ltd.). The cells were transfected at 70% confluence with 3 μg pLVX-shRNA2-Puro-mPrnp or pLVX-mPrnp-3flag-ZsGreen-Puro transfer plasmid, 2 μg of psPAX2, and 1 μg of pMD2.G in a ratio of 3:2:1 using PEI in Opti-MEM. After 48 h of incubation at 37˚C with 5% CO_2, fluorescence screening indicated a packaging efficiency of over 85%. To obtain stably transfected mGCs, lentiviral transduction was performed at the optimized multiplicity of infection (MOI) of 80, followed by selection with 3 μg/ml of puromycin for 72 h (cat. no. PS1224; Beijing Puxitang Biotechnology Co., Ltd.), and 1 μg/ml thereafter for culture maintenance. After 72 h of transduction, the infected mGCs were collected for subsequent experiments. Stable PrP^c-knockdown mGCs were established through lentiviral shRNA transduction. Following this, these cells were infected with a lentivirus designed to overexpress PrP^c, allowing for both the knockdown and overexpression of PrP^c within the same cellular environment.

Reverse transcription quantitative PCR (RT-qPCR). Total RNA was extracted from mGCs following the manufacturer's instructions (cat. no. UE-MN-MS-RNA-10; Suzhou UElandy Biotechnology Co., Ltd.). Quantity and purity of RNA were determined using a NanoDrop™ 2000 spectrophotometer (Thermo Scientific). The RNA concentrations were measured at A260, while the purity was evaluated by calculating the A260/A280 ratios. Subsequently, RT was performed following the manufacturer's instructions for the RevertAid™ Master Mix (cat. no. M1632; Thermo Fisher Scientific, Inc.). qPCR was carried out on a CFX Connect fluorescent Real-Time PCR System (Bio-Rad Laboratories, Inc.), using the Universal SYBR Green qPCR Supermix (cat. no. S2024L; US Everbright, Inc.). The thermocycling conditions were as follows: 95˚C for 5 min, followed by 45 cycles of 95˚C for 5 sec and 60˚C for 30 sec. The *PRNP* primer sequences (cat. no. MQP094390; GeneCopoeia, Inc.) were as follows: *PRNP* forward (F), 5'-GGCCCATGATCCATTTTGGC-3' and reverse (R), 5'-TGCTGTACTGATCCACTGGC-3'. Additionally, the following primer sequences were used for β-actin (Wuhan Servicebio Technology Co., Ltd.): β-actin F, 5'-GACTTTGTACATTGTTTTG-3' and R, 5'-TGCACTTTTATTGGTCTCA-3', which was selected as the internal control for normalization. The $2^{-\Delta\Delta Cq}$ method was employed for quantification of the data (20). qPCR was selected for its superior sensitivity in detecting transcript-level changes (detection threshold ≤10 copies/μl) compared with conventional PCR (21,22), with SYBR Green chemistry providing cost-effective quantification of *PRNP* expression dynamics.

Western blotting (WB). mGCs and ovarian tissue were lysed on ice for 30 min in RIPA buffer supplemented with protease inhibitors (cat. no. R0010; Beijing Solarbio Science & Technology Co., Ltd.). The total protein content was determined using a BCA Protein Quantification Kit (cat. no. C0050; TargetMol Chemicals Inc.). Following protein quantification, 25 μg total protein/lane in each sample were separated via 10% SWE Rapid High Resolution Running Buffer (cat. no. G2081-1L; Wuhan Servicebio Technology Co., Ltd.). Subsequently, the separated proteins were transferred onto PVDF membranes (cat. no. IPVH00010; MilliporeSigma).

To block non-specific binding, the PVDF membranes were incubated in a solution of 5% non-fat dried milk (cat. no. S10191; Beijing Puxitang Biotechnology Co., Ltd.) in Tris-buffered saline containing 0.1% Tween 20 (TBST; cat. no. T1082; Beijing Solarbio Science & Technology Co., Ltd.) for 2 h at room temperature. After blocking, the membranes were incubated overnight at 4˚C with the following primary antibodies: Anti-CD230 (Prion; cat. no. 808001; BioLegend, Inc.) and anti-β-actin at a 1:5,000 dilution (cat. no 20536-1-AP; Proteintech Group, Inc.).

After the overnight incubation, the membranes were washed three times with TBST and incubated for 2 h at room temperature with the following secondary antibodies:

HRP-conjugated goat anti-rabbit IgG at a 1:1,000 dilution (SA00001-2; Proteintech Group, Inc.) and HRP-conjugated goat anti-mouse IgG at a 1:10,000 dilution (SA00001-1; Proteintech Group, Inc.).

Finally, an enhanced chemiluminescence detection reagent (cat. no. S6009L; Suzhou UE Landi Biotechnology Co., Ltd.) was used to visualize the immunoreactive bands on ChemiDoc MP (Bio-Rad Laboratories, Inc.). Densitometry of the WB bands was performed using ImageJ 1.48V software (National Institutes of Health).

Apoptosis assay. Following the instructions of the Annexin V/PI detection Kit (cat. no. Y6026S; Suzhou UE Landy Biotechnology Co., Ltd.), $1x10^5$ mGCs were digested with 0.25% trypsinization solution (without EDTA)(cat. no. T1350; Beijing Solarbio Science & Technology Co., Ltd.), then enzymatically neutralized and resuspended in cold staining buffer, then resuspended in a staining buffer, which was prepared by adding 5 μl each Annexin V storage solution and 5 μl PI storage solution. Subsequently, the cells were incubated in the dark at 4˚C for 20 min and analyzed using a NovoCyte D3000 flow cytometer (Agilent Technologies, Inc.) Flow cytometry data were analyzed using De Novo FCS Express™ 6 software (Agilent Technologies, Inc.). Annexin V/PI dual staining was employed to differentiate early apoptotic (Annexin V^+/PI^-) from late apoptotic/necrotic (Annexin V^+/PI^+) populations, enabling stage-specific analysis of mGC death pathways, the total percentage of apoptotic cells reflects the overall measurement of both early and late apoptotic populations.

Cell cycle assay. For cell cycle analysis, $5x10^5$ mGCs were harvested by trypsinization at 72 h post-infection. The cells were then washed with cold PBS and fixed in 70% ice-cold ethanol at 4˚C overnight. Next, mGCs were incubated with RNase A and PI in a 0.5 ml reaction mixture (cat. no. C6031S; Suzhou UE Landy Biotechnology Co., Ltd.) at 37˚C for 30 min in a dark chamber. Cell cycle distribution was measured using a NovoCyte D3000 flow cytometer and analyzed with De Novo FCS Express™ 6 software (Agilent Technologies, Inc.).

ELISA for hormone measurements. mGC culture medium containing 10% FBS and mouse serum collected by centrifugation at 3,000 x g for 5 min at 4˚C were used to measure the concentrations of E_2 (cat. no. SEKM-0286; Beijing Solarbio Science & Technology Co., Ltd.), AMH (cat. no SEKM-0310; Beijing Solarbio Science & Technology Co., Ltd.), P4 (cat. no. SEKSM-0002; Beijing Solarbio Science & Technology Co., Ltd.), FSH (cat. no. KE1425; ImmunoWay Biotechnology Company) and luteinizing hormone (LH; cat. no. KE1421; ImmunoWay Biotechnology Company), following the manufacturer's instructions.

Animals. A total of 24 mice were used, comprising FVB-PRNP-/- and FVB wild-type (WT) mice, with each group consisting of 12 females. At the start of the experiment, the mice were 7 weeks old, and body weight was of 19.1-22.9 g (mean ± SD: 20.82±1.13 g). PRNP KO mice with an FVB genetic background were provided by Professor Wen-Quan Zou (Jiangxi Academy of Clinical Medical Sciences of the First Affiliated Hospital of Nanchang University) and Professor Li Cui (Department of Neurology, First Hospital of Jilin University). FVB WT mice, sourced from GemPharmatech Co. Ltd., were utilized as controls in the present study. All experimental protocols were approved by the Institutional Animal Care and Use Committee (IACUC) of the First Affiliated Hospital of Nanchang University (approval no. CDYFY-IACUC-202310QR030; Nanchang, China) in accordance with the National Institutes of Health Guidelines for animal welfare. To maintain optimal health and experimental integrity, both the KO and WT mice were housed in individually ventilated cages under specific pathogen-free (SPF) conditions, maintaining a temperature of 22±1˚C and humidity levels of 55±10%. They were kept on a 12:12-h light/dark cycle. The animals had unrestricted access to autoclaved standard rodent chow and reverse-osmosis purified water. These carefully controlled housing conditions minimized the potential influence of external pathogens on the experimental outcomes, ensuring that any observed differences between the KO and WT groups could be more accurately attributed to the genetic modifications rather than environmental factors. Breeding pairs were formed by housing WT and KO female mice (n=6 per group) with proven-fertility WT males at 10 weeks of age under specific pathogen-free conditions. After confirming the presence of copulatory plugs, which indicated successful mating and was designated as Gestational Day 0, the dams were individually housed in ventilated cages. Inhalant anesthesia was induced with 5% isoflurane (cat. no. R510-22-16; RWD Life Science Co., Ltd.) in oxygen at 1 l/min flow rate, and maintained for 5 min until the pedal withdrawal reflex ceased and the respiratory rate stabilized (40-60 breaths/min). Cervical dislocation was performed with simultaneous isoflurane overdose to ensure humane euthanasia. Death validation included confirmation of apnea for >3 min and absence of the corneal reflex. Terminal whole blood samples (~0.3 ml) were obtained via retro-orbital venous plexus puncture within 2 min post-mortem to ensure coagulation integrity. Ovarian tissues were dissected, fixed in 4% paraformaldehyde at 4˚C for 24-48 h, then processed for paraffin embedding and hematoxylin & eosin (H&E) staining.

H&E staining. H&E staining was performed in accordance with a standard protocol (23,24). Specifically, ovarian tissues were fixed in 4% paraformaldehyde (w/v in 0.1 M PBS, pH 7.4) at 4˚C for a duration of 24 to 48 h, 5-μm-thick paraffin sections underwent three 5-min immersions in xylene. This was followed by a rehydration process through a graded series of ethanol concentrations: 100, 95, 80, and 70% (v/v), with each step lasting 2 min, ultimately concluding in distilled water. Next, the sections were stained with H&E (cat. no. L110216041; Nanchang Yulu Experimental Equipment Co., Ltd.). Sections were stained with Mayer's hematoxylin at room temperature (23±2˚C) for a duration of 3 min, and this was followed by staining with eosin Y alcoholic solution at the same temperature for 2 min. Ovarian follicles were quantified using systematic random sampling in every sixth serial section with a thickness of 5 μm. A manual counting method was employed, examining 30 non-overlapping fields per ovary at a magnification of 200x using a light microscope (Beijing Sunny Instruments Co., Ltd.). Follicles were identified across

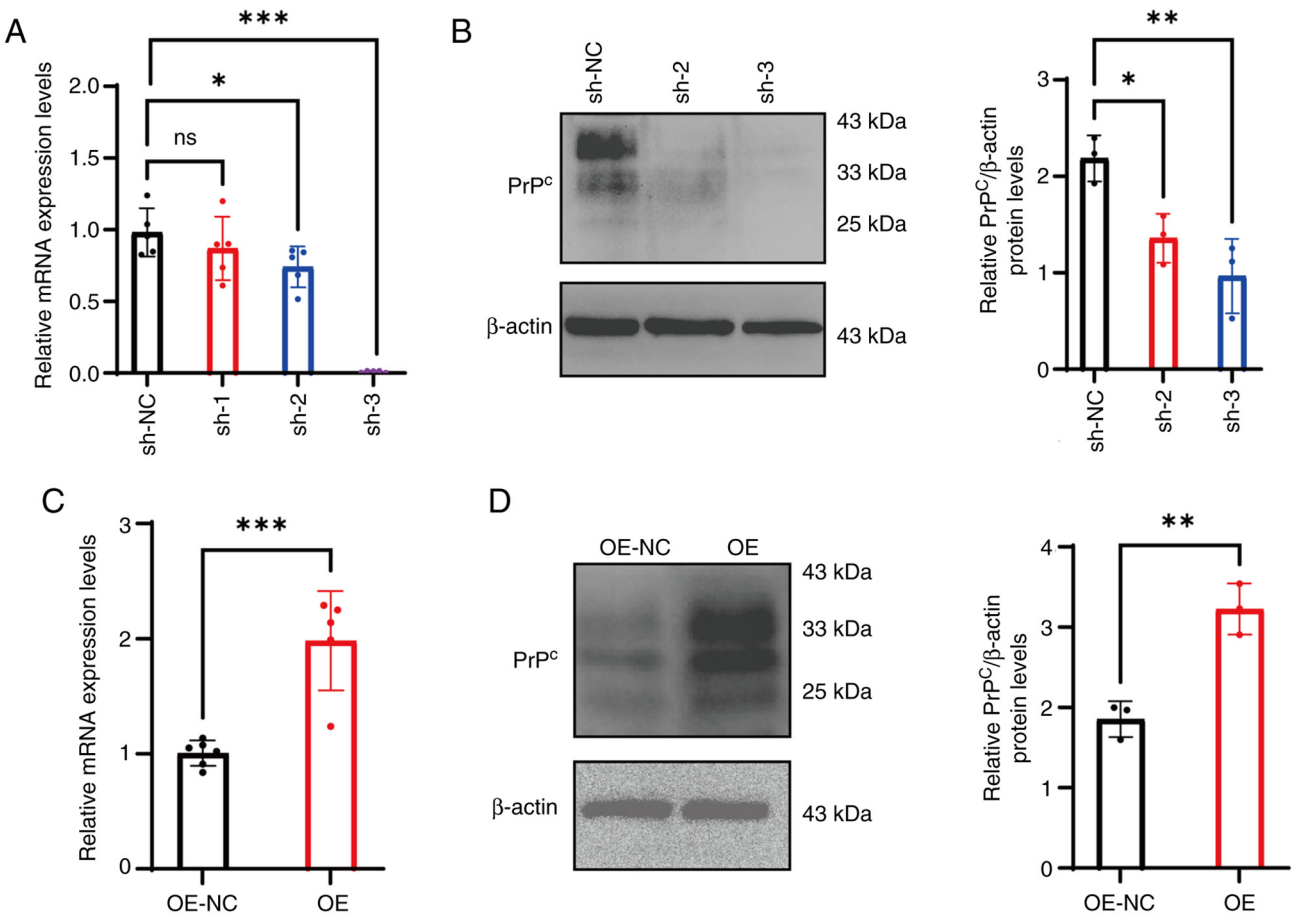

Figure 1. PrP^c knockdown and OE efficiency in mGCs. (A) mRNA expression levels of *PRNP* and (B) protein expression levels of PrP^c in mGCs transfected with different shRNAs. (C) mRNA expression levels of *PRNP* and (D) protein expression levels of PrP^c in mGCs transfected with OE vectors. β-actin was used as an internal control. *P<0.05; **P<0.01; ***P<0.001. ns, non-significant; PrP^c, cellular prion protein; *PRNP*, prion protein gene; mGCs, mouse ovarian granulosa cells; OE, overexpression; sh, short hairpin; NC, negative control.

various stages, from primordial to antral, in accordance with the Amsterdam Consensus Criteria (25,26).

Estrous cycle staging. Estrous cycle staging was performed through daily vaginal smear cytology between 9:00-10:00 a.m. Vaginal lavage samples were obtained using 10 μl sterile PBS, placed onto poly-L-lysine coated slides, and fixed in 4% paraformaldehyde at 4˚C for 15 min. Hematoxylin (3 min) and eosin (30 sec) staining at room temperature, adhering to standard protocols.

Statistical analysis. Data are presented as the mean ± SD based on a minimum of three independent experiments. Prior to analysis, normality was assessed using Shapiro-Wilk test (α=0.05) and the homogeneity of variance was confirmed via Brown-Forsythe test. Parametric tests were applied when assumptions were satisfied. Statistical analyses were carried out using GraphPad Prism 9.5 software (Dotmatics). For the comparison between two groups, a two-tailed unpaired Student's t-test was used, with Cohen's d effect sizes and 95% confidence intervals automatically calculated by the software. For the comparison of >2 groups, one-way ANOVA with Tukey's post hoc test (for all pairwise comparisons) or Dunnett's post hoc test (for comparisons vs. the control group) was applied, with partial η^2 effect sizes and family-wise error rate control at α=0.05. P<0.05 was considered to indicate a statistically significant difference.

Results

Validation of PrP^c knockdown and OE efficiency. To knock down PrP^c in mGCs, the following lentivirus-based vectors were used: m*PRNP* sh-1, sh-2 and sh-3. Compared with those of mGCs infected with the NC vector (sh-NC), the mRNA expression levels of *PRNP* in the sh-1 group exhibited no significant change (P>0.05). However, infections with sh-2 and sh-3 resulted in a marked reduction in mRNA expression (sh-2:P<0.05; Sh-3:P<0.001), respectively, confirming successful knockdown of the *PRNP* gene (Fig. 1A). Supporting these findings, WB analysis revealed that the gray values of the PrP^c protein bands in cells transfected with sh-2 and sh-3 were significantly reduced compared with those in the sh-NC group (P<0.05; Fig. 1B). Based on these results, sh-2 and sh-3 were selected as the most efficient shRNAs for subsequent experiments.

In the PrP^c OE group, the mRNA expression levels of *PRNP* were significantly increased compared with those in the OE-NC group (P<0.001; Fig. 1C), indicating that the OE vector effectively increased the transcription of the *PRNP* gene. Correspondingly, the expression levels of the PrP^c

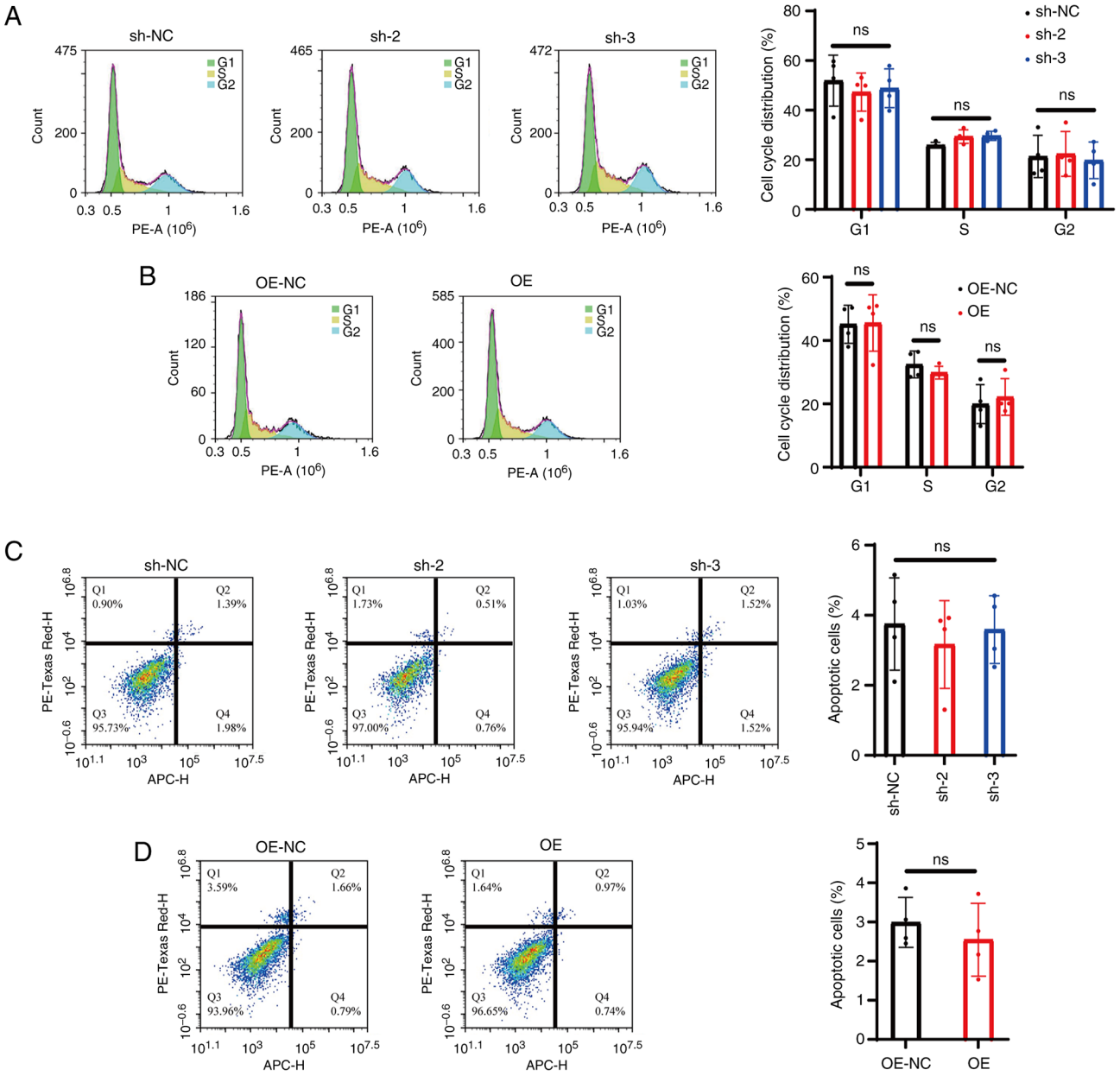

Figure 2. Cellular prion protein exhibits minimal influence on the cell cycle distribution and apoptosis of mouse granulosa cells. Flow cytometry was employed to analyze the cell cycle distribution, enabling quantification of cells in the G_0/G_1, S and G_2/M phases after transfection with (A) different shRNAs or (B) OE vectors. Apoptotic and necrotic cells were assessed using Annexin V/PI staining after transfection with (C) different shRNAs or (D) OE vectors. ns, non-significant; sh, short hairpin; NC, negative control; OE, overexpression.

protein in the OE group was significantly increased compared with that in the OE-NC group (P<0.01; Fig. 1D), aligning with the observed trend in mRNA expression levels.

PrP^c does not alter mGC cycle progression or apoptosis. Flow cytometry analysis was carried out to assess cell cycle distribution in mGCs. The results revealed no significant differences in the proportions of cells in the G_1, S and G_2 phases among the sh-2, sh-3 and sh-NC groups (P>0.05; Fig. 2A). Likewise, no notable changes were observed in the distribution of cells across these phases in the OE group compared with OE-NC (P>0.05; Fig. 2B).

Analysis of apoptosis using the Annexin V/PI double staining method by flow cytometry revealed that, under normal culture conditions, the apoptosis rate of mGCs was consistent between the sh-NC and OE-NC groups. Moreover, sh-2, sh-3 and sh-NC did not exhibit any significant differences in the proportion of apoptotic cells (P<0.05; Fig. 2C). Similarly, the OE group demonstrated no notable variation in the proportion of apoptotic cells compared with OE-NC (P<0.05; Fig. 2D).

PrP^c knockdown reduces AMH secretion while preserving P4 and E2 production in mGCs. AMH levels averaged 56.10±3.73 ng/ml in the sh-NC group, while they significantly decreased to 42.27±7.51 and 42.7±6.85 ng/ml in the sh-2 and sh-3 groups respectively (P<0.05; Fig. 3A). However, PrP^c expression was restored following knockdown in mGCs infected both with the *PRNP* knockdown and OE vectors (sh-2 + OE and sh-3 + OE; Fig. S1B), and AMH levels increased compared

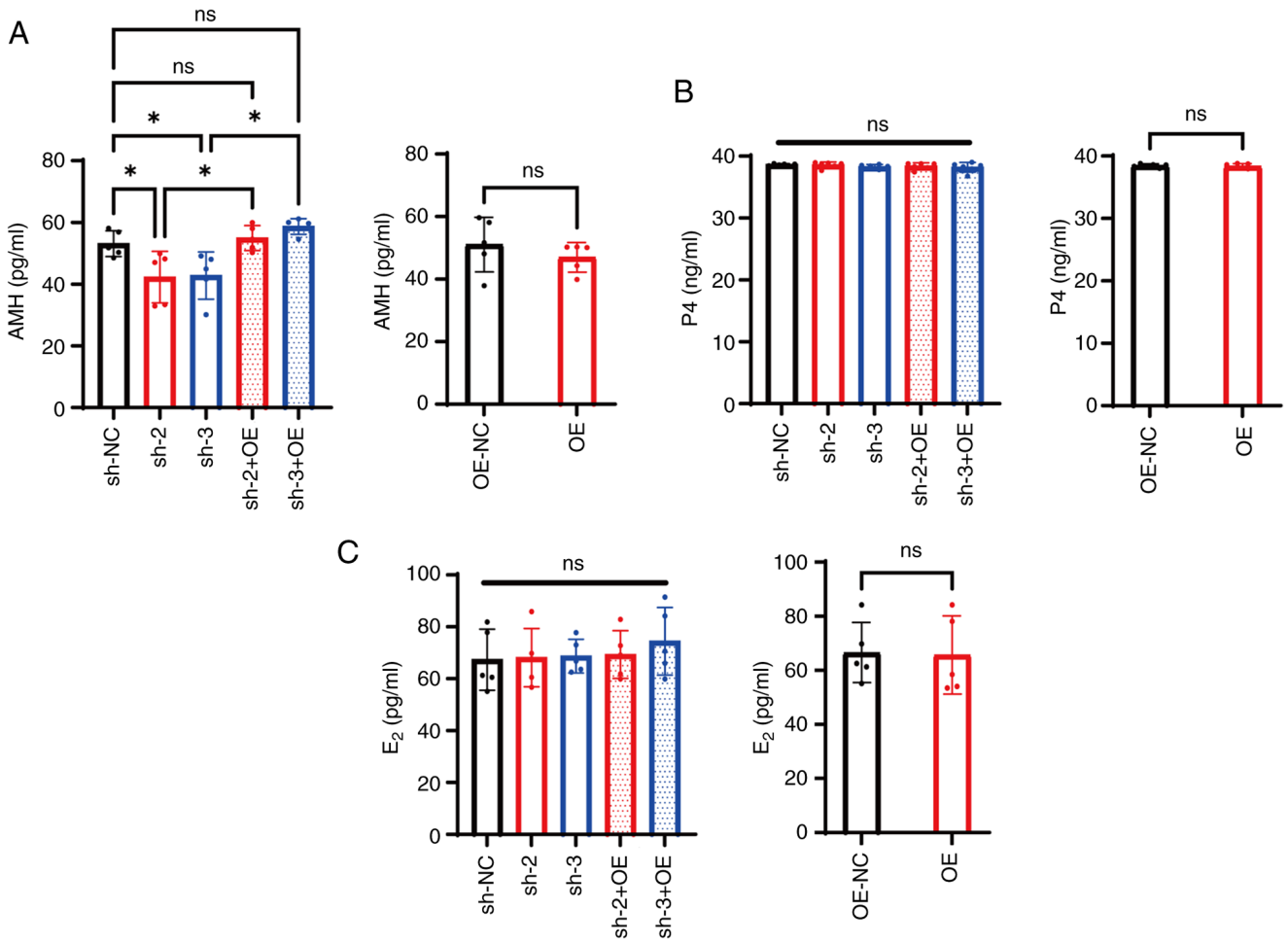

Figure 3. Cellular prion protein knockdown specifically reduces AMH secretion in mGCs. (A) AMH, (B) P4 and (C) E_2 levels in the culture medium of mGCs transfected with different shRNAs, OE vectors or their combination. *P<0.05. ns, non-significant; AMH, anti-Müllerian hormone; mGCs, mouse granulosa cells; P4, progesterone; E_2, estradiol; sh, short hairpin; OE, overexpression; NC, negative control.

with those in the sh-2 and sh-3 groups (P<0.05; Fig. 3A). By contrast, the average AMH expression levels in the OE group was 46.96±4.22 ng/ml, exhibiting no significant difference compared with that in the OE-NC group (P>0.05; Fig. 3A).

The average P4 level was 38.61±0.15 ng/ml in the sh-NC group, and 38.57±0.43 and 38.24±0.37 ng/ml in the sh-2 and sh-3 groups, respectively, with the latter showing no significant difference compared with the control group (P>0.05; Fig. 3B). Furthermore, compared with the sh-2 and sh-3 groups, the sh-2 + OE and sh-3 + OE groups did not exhibit significant changes in P4 levels (P>0.05; Fig. 3B). Similarly, the average P4 level in the OE group was 38.33±0.40 ng/ml, which was comparable with that in the OE-NC group (P>0.05; Fig. 3B).

The average E_2 level in the sh-NC group was 67.33±10.54 pg/ml, while the sh-2 and sh-3 groups exhibited values of 68.11±10.07 and 68.74±5.81 pg/ml, respectively, both showing no significant differences compared with sh-NC (P>0.05; Fig. 3C). Similarly, compared with the sh-2 and sh-3 groups, no notable changes in E_2 expression levels were observed in the sh-2 + OE and sh-3 + OE groups (P>0.05; Fig. 3C). Likewise, the average E_2 level in the OE group was 65.67±11.67 pg/ml, which was not significantly different compared with that in the OE-NC group (P>0.05; Fig. 3C).

PrP^c expression levels do not affect the classification count of ovaries. Ovaries from WT and KO mice were isolated and WB was carried out to assess PrP^c protein expression levels. The results indicated that PrP^c levels in the ovaries of KO mice were reduced compared with those in the WT group (Fig. 4A) confirming the effectiveness of the KO.

At 7 weeks of age, ovarian tissue was collected, and the wet weight index of ovaries was measured. The WT group had an ovarian weight of 0.390±0.08 mg/g, while the KO group exhibited a weight of 0.389±0.02 mg/g, with no statistically significant difference between the groups (P>0.05; Fig. 4B).

H&E staining revealed the pathological and morphological characteristics of the ovaries in each group (Fig. 4C). Although the KO group exhibited a slight reduction in the number of primordial and primary follicles, this difference was not statistically significant (P>0.05; Fig. 4D). Similarly, there were no significant differences in the numbers of secondary, antral or atretic follicles between the two groups (P>0.05; Fig. 4D).

PRNP deficiency elevates circulating FSH levels with unaltered AMH, LH and E_2 levels. FSH levels in KO mice were significantly increased at 6.64±0.68 ng/ml compared with 4.52±1.18 ng/ml in the WT group (P<0.01; Fig. 5A). By contrast, E_2 levels were not significantly different between the

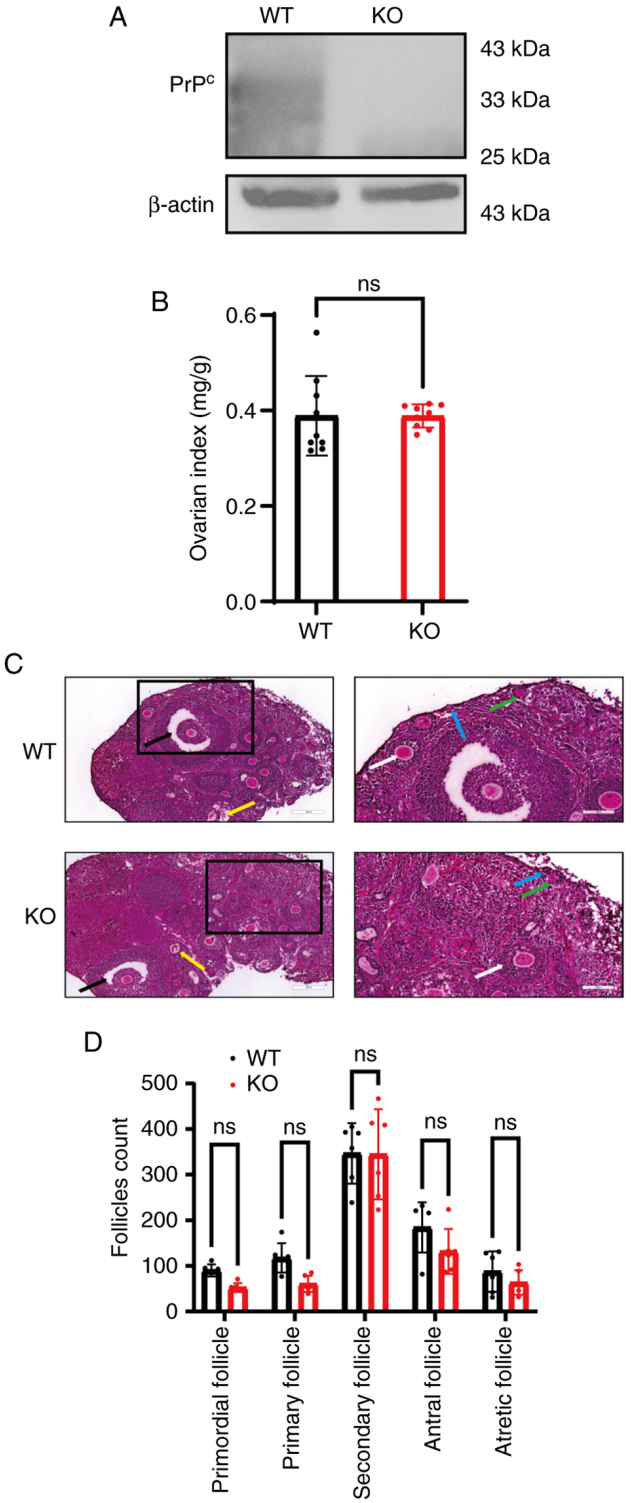

Figure 4. Prion protein gene KO mice exhibit normal ovarian morphology and follicular development. (A) PrP^c protein expression in the ovaries of WT and KO mice. (B) Ratio of bilateral ovary weight to body weight showed no differences between groups. (C) H&E staining on mouse ovaries (scale bars, 200 μm for overviews and 100 μm for higher mag). The stages of follicular development are clearly indicated by color-coded arrows: Blue represents primordial follicles, which consist of a single layer of squamous granulosa cells; green denotes primary follicles, characterized by cuboidal granulosa cells; white signifies secondary follicles, identifiable by having ≥3 layers of granulosa cells and the early formation of an antrum; black marks antral follicles, distinguished by the presence of a fluid-filled cavity; and yellow indicates atretic follicles, which display pyknotic granulosa cell nuclei and fragmentation of the zona pellucida. (D) Follicle counts across developmental stages were comparable between WT and KO mice. ns, non-significant; WT, wild-type; KO, knockout; PrP^c, cellular prion protein.

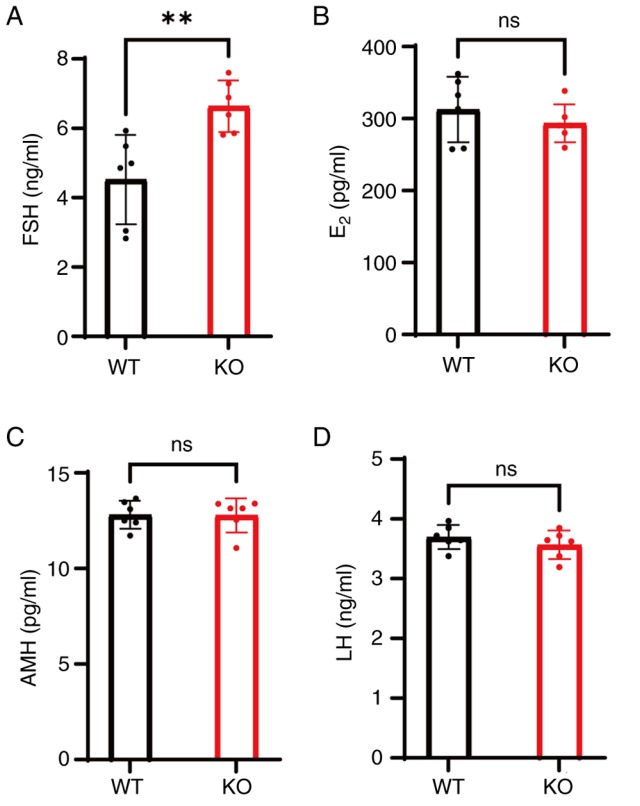

Figure 5. KO mice exhibit elevated FSH levels but normal E_2, AMH and LH levels. Serum hormone levels of (A) FSH, (B) E_2, (C) AMH and (D) LH in WT and KO mice. **P<0.01. ns, non-significant; FSH, follicle-stimulating hormone; LH, luteinizing hormone; E_2, estradiol; AMH, anti-Müllerian hormone; WT, wild-type; KO, knockout.

two groups (P>0.05; Fig. 5B). Similarly, AMH and LH levels were also not significantly different between WT and KO mice (P>0.05; Fig. 5C and D).

PRNP KO mice exhibit normal reproductive performance. WT and KO mice exhibited a standard estrous cycle, typically spanning 4-5 days per cycle and encompassing four distinct phases: Proestrus, estrus, metestrus and diestrus (Fig. 6A). In the proestrus stage (P), the smears are primarily made up of nucleated epithelial cells, which are characterized by their polygonal shape, large spherical nuclei, and abundant cytoplasm. As the cycle progresses to estrus (E), there is a notable increase in keratinized epithelial cells, which display a distinct eosinophilic staining in their cytoplasm. This is followed by metestrus (M), where the number of keratinized cells begins to decline, and nucleated epithelial cells become more present, accompanied by a few clusters of leukocytes. Finally, in the diestrus stage, the cytological composition shifts to predominantly leukocytes, with few scattered nucleated epithelial cells present (27). Each stage in the WT mice was clearly defined, with smooth and consistent transitions between phases. Similarly, KO mice exhibited no notable alterations in cycle duration, with neither a marked prolongation nor a noticeable shortening of the cycle observed (Fig. 6B).

No statistically significant differences were observed in the litter intervals between the two groups (P>0.05; Fig. 6C). The average litter size remained consistent at 8-10 pups, and the mothers exhibited normal nurturing abilities. The offspring

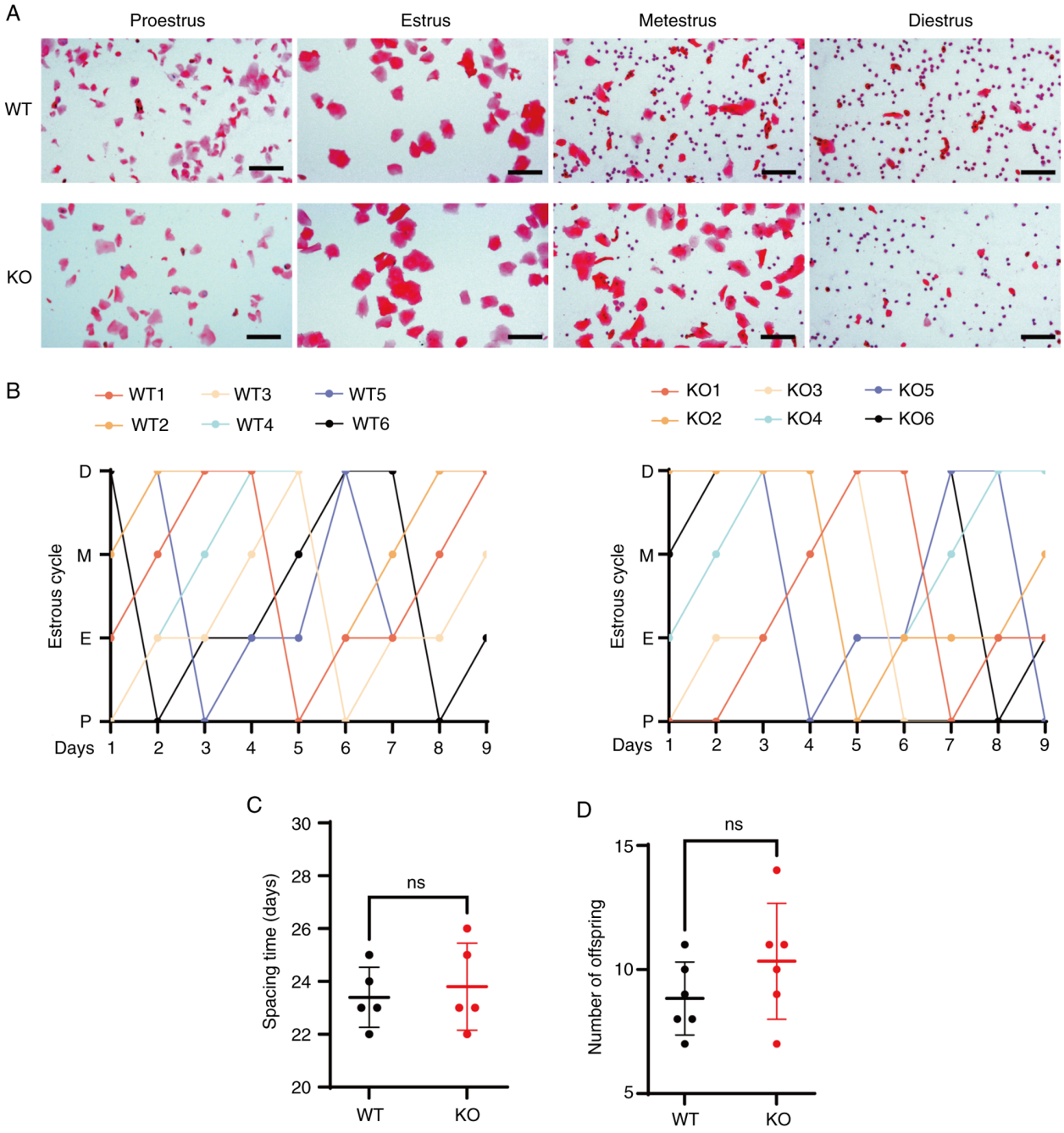

Figure 6. KO mice exhibit regular estrous cycle and fertility. (A) Vaginal secretion smears stained with H&E stain during estrous cycle phases: Proestrus, estrus, metestrus, diestrus (scale bar, 50 μm). (B) Regular estrous cycle patterns in mice spanning 9 consecutive days. (C) Interval from mating, following co-housing, to parturition. (D) Number of offspring at birth. ns, non-significant; WT, wild-type; KO, knockout; P, proestrus; E, estrus; M, metestrus; D, diestrus.

survival rate was high, with no notable differences detected between the groups (P>0.05; Fig. 6D).

Discussion

Previous studies have predominantly explored the role of PrP^c within the nervous system (28-31). However, there is little research on the function of PrP^c in non-neuronal tissues, especially in endocrine regulation. The present *in vitro* study revealed that PrP^c can selectively affect the secretion of AMH, while no significant changes in AMH, P4, E_2, folliculogenesis and the reproductive cyclicity in mice. These findings broaden the functional range of PrP^c beyond its typical roles in neuroprotection and synaptic plasticity (32,33), indicating that PrP^c may be a potential niche regulator of ovarian reserve biomarkers.

The present study revealed that alterations in the expression of PrP^c in mGCs did not significantly influence the cell cycle or apoptosis, suggesting that PrP^c may not regulate cellular homeostasis in mGCs. PrP^c may not directly affect the signaling molecules involved in key cell cycle transitions, such as those between the G_1/S and G_2/M phases. However, its role varies significantly in other systems. In neural environments, PrP^c acts as an accelerator of apoptosis during proteotoxic stress by impairing the ESCRT-0/AMPAR axis. In renal settings, it promotes regeneration through the activation of the PI3K/Akt-mTOR pathway. In cardiac contexts, PrP^c is

crucial for structural recovery, although it does not influence functional recovery. Additionally, in oncogenic environments, it serves as a key regulator of cell fate by modulating the dynamics between p53 and MDM2 during endoplasmic reticulum stress (34-36). Additionally, a previous study has highlighted the presence of compensatory mechanisms among members of the prion protein family, particularly PrP^c and Shadoo, which aid in maintaining cell cycle progression and suppressing apoptosis (37).

The levels of AMH, which is considered a marker of the ovarian reserve function and is primarily secreted by GCs (15), were decreased when PrP^c was knocked down. The effect of PrP^c knockdown may be associated with disrupted TGF-β/bone morphogenetic protein (BMP)-SMAD superfamily signaling pathways (38). AMH transcription is strictly controlled by SMAD1/5/8 complexes, which are activated by BMP ligands (39). The present findings are consistent with mechanistic framework proposed by Puig *et al* (40), which suggests that PrP^c plays a role in modulating the trafficking of FSHR and bone morphogenetic protein receptors (BMPR-II). Regarding the secretion of P4 and E_2, no significant changes were observed after PrP^c knockdown or overexpression, and the AMH-specific effect contrasts those of classical steroidogenic regulators, such as PPAR-γ agonists, miR-335-5p, retinoic acid, and artemisinins, which alter multiple hormonal axes (41-44). It may be hypothesized that PrP^c stabilizes BMP receptor clusters on GCs, which activates SMAD phosphorylation and subsequent AMH synthesis. This hypothesis can be tested by mapping the interactions between PrP^c and BMP receptor 2 and by quantifying the levels of phosphorylated-SMAD1/5 in PrP^c knockdown models.

The results of the present study indicating that PrP^c is dispensable for murine ovarian function contrasts with its reported roles in neuronal survival, underscoring profound tissue specificity (45). Although PrP^c deletion in neurons induces apoptosis via Bcl-2 suppression, GCs may remain viable after PrP^c depletion through compensatory mechanisms involving the Shadoo protein (46).

Despite minor changes, no statistically significant differences were observed in the ovary weight and the numbers of primordial and primary follicles in the PrP^c KO mice compared with the WT group. Furthermore, there seemed to be no evident changes in the estrous cycle, litter interval or the number of pups per litter between the two groups. This suggests that PrP^c may not be critical in maintaining the structure and reproductive activity of the ovaries. Vigorous compensatory mechanisms in the organism may have abolished the effect of PrP^c deficiency on ovarian function.

Furthermore, the lack of PrP^c does not seem to interfere with the estrous cycle or the reproductive functions, potentially because the hormonal regulatory pathways within the hypothalamic-pituitary-ovarian axis maintain normal reproductive rhythms and functions (47). Nonetheless, it cannot be ruled out that, under chemotherapy-induced ovarian damage or under hyperandrogenic conditions mimicking polycystic ovary syndrome (PCOS), PrP^c may have a key impact on reproductive functions.

The mouse model used in the present study may not capture all the physiological and pathological intricacies of the human ovary. There are marked differences in the structural, functional and hormonal regulation, as well as the reproductive cycle between mouse and human ovaries. For example, folliculogenesis in humans is a process that spans 90 to 120 days, which is significantly longer than the 14 to 21-day cycle observed in mice. In humans, primordial follicles can remain dormant for several decades, a situation that can contribute to oxidative stress within the ovarian environment. Additionally, humans typically exhibit a single-wave, monovulatory pattern for the selection of the dominant follicle, in contrast to mice, which display multi-wave, polyovulatory cycles (48). In addition, there is an apparent limitation to the *in vitro* cell culture model used in the present study, since cultured cells may lose some of their physiological characteristics (49,50) and be affected by microenvironmental conditions (51,52), which may result in findings that do not represent the *in vivo* settings. Murine ovaries lack the protracted folliculogenesis and hormonal complexity of humans. Furthermore, environmental endocrine disruptors such as phthalates (53), which potently alter human AMH levels, were not examined in the present study.

PRNP KO mice seem to have phenotypic resilience, but this does not entirely invalidate their clinical relevance. Under stress, there can be a compensatory failure and PrP^c may have a key effect on ovarian function. In mice, Shadoo-mediated compensatory mechanisms may take place (54), whilst in humans these mechanisms may not occur. When humans face prolonged oxidative stress, for example during chemotherapy or when there is age-related follicular depletion, Shadoo-mediated redundancy may not be sufficient. The observation of elevated (FSH) levels in PRNP knockout (KO) mice aligns with the clinical characteristic of increased early-follicular phase FSH levels seen in patients diagnosed with diminished ovarian reserve (DOR), as defined by established international diagnostic criteria (55). Additionally, PrP^c expression in human follicular fluid may be associated with AMH levels or *in vitro* fertilization outcomes; therefore, cohort studies examining the association between PrP^c concentrations in human follicular fluid and key reproductive parameters is warranted are warranted.

The anti-apoptotic role of PrP^c in glioma cells via interaction with PRKC Apoptosis WT1 Regulator (PAWR) raises the possibility that PrP^c may protect GCs from chemotherapy-specific observations in glioma models (56). This hypothesis aligns with clinical observations that the ovarian reserve declines post-chemotherapy (57-59), it was hypothesized that PrP^c expression critically regulates chemotherapy-induced ovarian reserve depletion by modulating granulosa cell survival pathways. Inhibiting PrP^c-PAWR interactions may sensitize ovarian cancer cells to chemotherapy while preserving normal ovarian tissue. Conversely, enhancing PrP^c activity could protect ovarian follicles during oncotherapy.

In conclusion, the present study revealed that PrP^c selectively disrupted AMH secretion in mGCs without affecting the levels of P4 and E_2 or the reproductive cycle. Unlike its anti-apoptotic roles in neurons or glioma, the role of PrP^c in AMH regulation was independent of cell survival. It was hypothesized that: Murine ovaries may exhibit compensatory mechanisms via Shadoo in the absence of PrP^c, while human cells exposed to prolonged stress, such as chemotherapy, may rely more on PrP^c for the regulation of AMH levels and cell survival. Clinically, PrP^c could refine ovarian reserve diagnostics or inspire fertility preservation strategies. Furthermore, targeting the PrP^c-BMP-SMAD interactions may also address

AMH dysregulation in polycystic ovary syndrome or ovarian insufficiency.

Acknowledgements

The authors would like to thank Professor Wen-Quan Zou (Jiangxi Academy of Clinical Medical Sciences of the First Affiliated Hospital of Nanchang University, Nanching, China), for technical discussion. The authors would also like to thank Professor Li Cui (Department of Neurology, First Hospital of Jilin University, Changchun. China) for their donation of FVB-*PRNP* tm1/ILAS congenic mice.

Funding

The present study was partially supported by the National Natural Science Foundation of China (grant no. 82260295).

Availability of data and materials

The data generated in the present study may be requested from the corresponding author.

Authors' contributions

CT interpreted data and revised the manuscript. QC and HW, who made contributions to the study's conceptualization and data validation. *In vivo* investigations, including surgical procedures and H&E staining, were carried out by QC, JH, and YW. QC, FL, TD and XY performed experiments. QY contributed to pathological assessments and the drafting of the manuscript. QC and HW confirm the authenticity of all the raw data. All authors participated in data analysis, manuscript review and they collectively assume accountability for the published work. All authors read and approved the final manuscript.

Ethics approval and consent to participate

The experimental procedures in the present study were approved by the Institutional Animal Care and Use Committee of The First Affiliated Hospital of Nanchang University (approval no. CDYFY-IACUC-202310QR030; Nanchang, China).

Patient consent for publication

Not applicable.

Competing interests

The authors declare that they have no competing interests.

References

1. Ermonval M, Petit D, Le Duc A, Kellermann O and Gallet PF: Glycosylation-related genes are variably expressed depending on the differentiation state of a bioaminergic neuronal cell line: Implication for the cellular prion protein. Glycoconj J 26: 477-493, 2009.
2. Hu W, Nessler S, Hemmer B, Eagar TN, Kane LP, Leliveld SR, Müller-Schiffmann A, Gocke AR, Lovett-Racke A, Ben LH, *et al*: Pharmacological prion protein silencing accelerates central nervous system autoimmune disease via T cell receptor signalling. Brain 133: 375-388, 2010.
3. Wulf MA, Senatore A and Aguzzi A: The biological function of the cellular prion protein: An update. BMC Biol 15: 34, 2017.
4. Watts JC, Bourkas MEC and Arshad H: The function of the cellular prion protein in health and disease. Acta Neuropathol 135: 159-178, 2018.
5. Sigurdson CJ, Bartz JC and Glatzel M: Cellular and molecular mechanisms of prion disease. Annu Rev Pathol 14: 497-516, 2019.
6. Ribes JM, Patel MP, Halim HA, Berretta A, Tooze SA and Klöhn PC: Prion protein conversion at two distinct cellular sites precedes fibrillisation. Nat Commun 14: 8354, 2023.
7. Salvesen Ø, Tatzelt J and Tranulis MA: The prion protein in neuroimmune crosstalk. Neurochem Int 130: 104335, 2019.
8. Dematteis G, Restelli E, Vanella VV, Manfredi M, Marengo E, Corazzari M, Genazzani AA, Chiesa R, Lim D and Tapella L: Calcineurin controls cellular prion protein expression in mouse astrocytes. Cells 11: 609, 2022.
9. Goedert M: NEURODEGENERATION. Alzheimer's and Parkinson's diseases: The prion concept in relation to assembled Aβ, tau, and α-synuclein. Science 349: 1255555, 2015.
10. Stoner A, Fu L, Nicholson L, Zheng C, Toyonaga T, Spurrier J, Laird W, Cai Z and Strittmatter SM: Neuronal transcriptome, tau and synapse loss in Alzheimer's knock-in mice require prion protein. Alzheimers Res Ther 15: 201, 2023.
11. Evoniuk JM, Johnson ML, Borowicz PP, Caton JS, Vonnahme KA, Reynolds LP, Taylor JB, Stoltenow CL, O'Rourke KI and Redmer DA: Effects of nutrition and genotype on prion protein (PrPC) gene expression in the fetal and maternal sheep placenta. Placenta 29: 422-428, 2008.
12. Moldenhauer LM, Jin M, Wilson JJ, Green ES, Sharkey DJ, Salkeld MD, Bristow TC, Hull ML, Dekker GA and Robertson SA: Regulatory T cell proportion and phenotype are altered in women using oral contraception. Endocrinology 163: bqac098, 2022.
13. Memon S, Li G, Xiong H, Wang L, Liu XY, Yuan M, Deng W and Xi D: Deletion/insertion polymorphisms of the prion protein gene (PRNP) in gayal (Bos frontalis). J Genet 97: 1131-1138, 2018.
14. Johnson ML, Grazul-Bilska AT, Reynolds LP and Redmer DA: Prion (PrPC) expression in ovine uteroplacental tissues increases after estrogen treatment of ovariectomized ewes and during early pregnancy. Reproduction 148: 1-10, 2014.
15. Buratini J, Dellaqua TT, Dal Canto M, La Marca A, Carone D, Mignini Renzini M and Webb R: The putative roles of FSH and AMH in the regulation of oocyte developmental competence: From fertility prognosis to mechanisms underlying age-related subfertility. Hum Reprod Update 28: 232-254, 2022.
16. Suarez-Henriques P, Miranda E Silva-Chaves C, Cardoso-Leite R, Guilermo-Ferreira R, Katiki LM and Louvandini H: Exploring AMH levels, homeostasis parameters, and ovarian primordial follicle activation in pubertal infected sheep on a high-protein diet. Res Vet Sci 169: 105158, 2024.
17. Smith ER, Ye D, Luo S, Xu IRL and Xu XX: AMH regulates a mosaic population of AMHR2-positive cells in the ovarian surface epithelium. J Biol Chem 300: 107897, 2024.
18. Xiang Y, Jiang L, Gou J, Sun Y, Zhang D, Xin X, Song Z and Huang J: Chronic unpredictable mild stress-induced mouse ovarian insufficiency by interrupting lipid homeostasis in the ovary. Front Cell Dev Biol 10: 933674, 2022.
19. Rios JS, Greenwood EA, Pavone MEG, Cedars MI, Legro RS, Diamond MP, Santoro N, Sun F, Robinson RD, Christman G, *et al*: Associations between anti-mullerian hormone and cardiometabolic health in reproductive age women are explained by body mass index. J Clin Endocrinol Metab 105: e555-e563, 2020.
20. Livak KJ and Schmittgen TD: Analysis of relative gene expression data using real-time quantitative PCR and the 2(-Delta Delta C(T)) method. Methods 25: 402-408, 2001.
21. Remans T, Keunen E, Bex GJ, Smeets K, Vangronsveld J and Cuypers A: Reliable gene expression analysis by reverse transcription-quantitative PCR: Reporting and minimizing the uncertainty in data accuracy. Plant Cell 26: 3829-3837, 2014.
22. Hatakeyama D, Chikamoto N, Fujimoto K, Kitahashi T and Ito E: Comparison between relative and absolute quantitative real-time PCR applied to single-cell analyses: Transcriptional levels in a key neuron for long-term memory in the pond snail. PLoS One 17: e0279017, 2022.
23. Salido J, Vallez N, González-López L, Deniz O and Bueno G: Comparison of deep learning models for digital H&E staining from unpaired label-free multispectral microscopy images. Comput Methods Programs Biomed 235: 107528, 2023.

24. Asaf MZ, Salam AA, Khan S, Musolff N, Akram MU and Rao B: E-Staining DermaRepo: H&E whole slide image staining dataset. Data Brief 57: 110997, 2024.
25. Egbert JR, Fahey PG, Reimer J, Owen CM, Evsikov AV, Nikolaev VO, Griesbeck O, Ray RS, Tolias AS and Jaffe LA: Follicle-stimulating hormone and luteinizing hormone increase Ca2+ in the granulosa cells of mouse ovarian follicles†. Biol Reprod 101: 433-444, 2019.
26. Kim SJ, Kim TE and Jee BC: Impact of imatinib administration on the mouse ovarian follicle count and levels of intra-ovarian proteins related to follicular quality. Clin Exp Reprod Med 49: 93-100, 2022.
27. Wall EG, Desai R, Khant Aung Z, Yeo SH, Grattan DR, Handelsman DJ and Herbison AE: Unexpected plasma gonadal steroid and prolactin levels across the mouse estrous cycle. Endocrinology 164: bqad070, 2023.
28. Abrams J, Arhar T, Mok SA, Taylor IR, Kampmann M and Gestwicki JE: Functional genomics screen identifies proteostasis targets that modulate prion protein (PrP) stability. Cell Stress Chaperones 26: 443-452, 2021.
29. Schmitt-Ulms G, Mehrabian M, Williams D and Ehsani S: The IDIP framework for assessing protein function and its application to the prion protein. Biol Rev Camb Philos Soc 96: 1907-1932, 2021.
30. Sawaya MR, Hughes MP, Rodriguez JA, Riek R and Eisenberg DS: The expanding amyloid family: Structure, stability, function, and pathogenesis. Cell 184: 4857-4873, 2021.
31. Lawrence JA, Aguilar-Calvo P, Ojeda-Juárez D, Khuu H, Soldau K, Pizzo DP, Wang J, Malik A, Shay TF, Sullivan EE, *et al*: Diminished neuronal ESCRT-0 function exacerbates AMPA receptor derangement and accelerates prion-induced neurodegeneration. J Neurosci 43: 3970-3984, 2023.
32. Lidón L, Vergara C, Ferrer I, Hernández F, Ávila J, Del Rio JA and Gavín R: Tau protein as a new regulator of cellular prion protein transcription. Mol Neurobiol 57: 4170-4186, 2020.
33. Ribeiro LW, Pietri M, Ardila-Osorio H, Baudry A, Boudet-Devaud F, Bizingre C, Arellano-Anaya ZE, Haeberlé AM, Gadot N, Boland S, *et al*: Titanium dioxide and carbon black nanoparticles disrupt neuronal homeostasis via excessive activation of cellular prion protein signaling. Part Fibre Toxicol 19: 48, 2022.
34. Yang CC, Sung PH, Chen KH, Chai HT, Chiang JY, Ko SF, Lee FY and Yip HK: Valsartan- and melatonin-supported adipose-derived mesenchymal stem cells preserve renal function in chronic kidney disease rat through upregulation of prion protein participated in promoting PI3K-Akt-mTOR signaling and cell proliferation. Biomed Pharmacother 146: 112551, 2022.
35. Sheu JJ, Chai HT, Chiang JY, Sung PH, Chen YL and Yip HK: Cellular prion protein is essential for myocardial regeneration but not the recovery of left ventricular function from apical ballooning. Biomedicines 10: 167, 2022.
36. Tuğrul B, Balcan E, Öztel Z, Çöllü F and Gürcü B: Prion protein-dependent regulation of p53-MDM2 crosstalk during endoplasmic reticulum stress and doxorubicin treatments might be essential for cell fate in human breast cancer cell line, MCF-7. Exp Cell Res 429: 113656, 2023.
37. Pimenta JMBGA, Pires VMR, Nolasco S, Castelo-Branco P, Marques CC, Apolónio J, Azevedo R, Fernandes MT, Lopes-da-Costa L, Prates J and Pereira RMLN: Post-transcriptional silencing of Bos taurus prion family genes and its impact on granulosa cell steroidogenesis. Biochem Biophys Res Commun 598: 95-99, 2022.
38. Hart KN, Stocker WA, Nagykery NG, Walton KL, Harrison CA, Donahoe PK, Pépin D and Thompson TB: Structure of AMH bound to AMHR2 provides insight into a unique signaling pair in the TGF-β family. Proc Natl Acad Sci USA 118: e2104809118, 2021.
39. Spector I, Derech-Haim S, Boustanai I, Safrai M and Meirow D: Anti-Müllerian hormone signaling in the ovary involves stromal fibroblasts: A study in humans and mice provides novel insights into the role of ovarian stroma. Hum Reprod 39: 2551-2564, 2024.
40. Puig B, Altmeppen HC, Linsenmeier L, Chakroun K, Wegwitz F, Piontek UK, Tatzelt J, Bate C, Magnus T and Glatzel M: GPI-anchor signal sequence influences PrPC sorting, shedding and signalling, and impacts on different pathomechanistic aspects of prion disease in mice. PLoS Pathog 15: e1007520, 2019.
41. Suriyakalaa U, Ramachandran R, Doulathunnisa JA, Aseervatham SB, Sankarganesh D, Kamalakkannan S, Kadalmani B, Angayarkanni J, Akbarsha MA and Achiraman S: Upregulation of Cyp19a1 and PPAR-γ in ovarian steroidogenic pathway by Ficus religiosa: A potential cure for polycystic ovary syndrome. J Ethnopharmacol 267: 113540, 2021.
42. Zhang S, Liu Y, Wang M, Ponikwicka-Tyszko D, Ma W, Krentowska A, Kowalska I, Huhtaniemi I, Wolczynski S, Rahman NA and Li X: Role and mechanism of miR-335-5p in the pathogenesis and treatment of polycystic ovary syndrome. Transl Res 252: 64-78, 2023.
43. Cai S, Chen M, Xue B, Zhu Z, Wang X, Li J, Wang H, Zeng X, Qiao S and Zeng X: Retinoic acid enhances ovarian steroidogenesis by regulating granulosa cell proliferation and MESP2/STAR/CYP11A1 pathway. J Adv Res 58: 163-173, 2024.
44. Liu Y, Jiang JJ, Du SY, Mu LS, Fan JJ, Hu JC, Ye Y, Ding M, Zhou WY, Yu QH, *et al*: Artemisinins ameliorate polycystic ovarian syndrome by mediating LONP1-CYP11A1 interaction. Science 384: eadk5382, 2024.
45. Doeppner TR, Kaltwasser B, Schlechter J, Jaschke J, Kilic E, Bähr M, Hermann DM and Weise J: Cellular prion protein promotes post-ischemic neuronal survival, angioneurogenesis and enhances neural progenitor cell homing via proteasome inhibition. Cell Death Dis 6: e2024, 2015.
46. Passet B, Castille J, Makhzami S, Truchet S, Vaiman A, Floriot S, Moazami-Goudarzi K, Vilotte M, Gaillard AL, Helary L, *et al*: The Prion-like protein Shadoo is involved in mouse embryonic and mammary development and differentiation. Sci Rep 10: 6765, 2020.
47. Lonardo MS, Cacciapuoti N, Guida B, Di Lorenzo M, Chiurazzi M, Damiano S and Menale C: Hypothalamic-ovarian axis and adiposity relationship in polycystic ovary syndrome: Physiopathology and therapeutic options for the management of metabolic and inflammatory aspects. Curr Obes Rep 13: 51-70, 2024.
48. Telfer EE, Grosbois J, Odey YL, Rosario R and Anderson RA: Making a good egg: Human oocyte health, aging, and in vitro development. Physiol Rev 103: 2623-2677, 2023.
49. Park SU, Walsh L and Berkowitz KM: Mechanisms of ovarian aging. Reproduction 162: R19-R33, 2021.
50. Amadei G, Handford CE, Qiu C, De Jonghe J, Greenfeld H, Tran M, Martin BK, Chen DY, Aguilera-Castrejon A, Hanna JH, *et al*: Embryo model completes gastrulation to neurulation and organogenesis. Nature 610: 143-153, 2022.
51. Chap BS, Rayroux N, Grimm AJ, Ghisoni E and Dangaj Laniti D: Crosstalk of T cells within the ovarian cancer microenvironment. Trends Cancer 10: 1116-1130, 2024.
52. Schoutrop E, Moyano-Galceran L, Lheureux S, Mattsson J, Lehti K, Dahlstrand H and Magalhaes I: Molecular, cellular and systemic aspects of epithelial ovarian cancer and its tumor microenvironment. Semin Cancer Biol 86: 207-223, 2022.
53. Mariana M, Castelo-Branco M, Soares AM and Cairrao E: Phthalates' exposure leads to an increasing concern on cardiovascular health. J Hazard Mater 457: 131680, 2023.
54. Pepe A, Avolio R, Matassa DS, Esposito F, Nitsch L, Zurzolo C, Paladino S and Sarnataro D: Regulation of sub-compartmental targeting and folding properties of the Prion-like protein Shadoo. Sci Rep 7: 3731, 2017.
55. Steiner AZ, Pritchard D, Stanczyk FZ, Kesner JS, Meadows JW, Herring AH and Baird DD: Association between biomarkers of ovarian reserve and infertility among older women of reproductive age. JAMA 318: 1367-1376, 2017.
56. Zhuang D, Liu Y, Mao Y, Gao L, Zhang H, Luan S, Huang F and Li Q: TMZ-induced PrPc/par-4 interaction promotes the survival of human glioma cells. Int J Cancer 130: 309-318, 2012.
57. Spears N, Lopes F, Stefansdottir A, Rossi V, De Felici M, Anderson RA and Klinger FG: Ovarian damage from chemotherapy and current approaches to its protection. Hum Reprod Update 25: 673-693, 2019.
58. Park HS, Seok J, Cetin E, Ghasroldasht MM, Liakath Ali F, Mohammed H, Alkelani H and Al-Hendy A: Fertility protection: A novel approach using pretreatment with mesenchymal stem cell exosomes to prevent chemotherapy-induced ovarian damage in a mouse model. Am J Obstet Gynecol 231: 111.e1-111.e18, 2024.
59. Guo Y, Xue L, Tang W, Xiong J, Chen D, Dai Y, Wu C, Wei S, Dai J, Wu M and Wang S: Ovarian microenvironment: Challenges and opportunities in protecting against chemotherapy-associated ovarian damage. Hum Reprod Update 30: 614-647, 2024.

Copyright © 2025 Cao et al. This work is licensed under a Creative Commons Attribution-NonCommercial-NoDerivatives 4.0 International (CC BY-NC-ND 4.0) License.